An investigation of magnetic reversal in submicron-scale Co dots using first order reversal curve diagrams

Chris Pike[a)]
Department of Geology, University of California, Davis, California 95616

Andres Fernandez[b)]
Lawrence Livermore National Laboratory, Livermore, California 94551

(Received 2 November 1998; accepted for publication 1 February 1999)

First order reversal curve (FORC) diagrams are a powerful method of investigating the physical mechanisms giving rise to hysteresis in magnetic systems. We have acquired FORC diagrams for an array of submicron-scale Co dots fabricated by interference lithography. These dots reverse magnetization through the nucleation and annihilation of a single-vortex state. Using FORC diagrams, we are able to obtain precise values for the nucleation and annihilation fields involved in magnetic reversal. Our results indicate, however, that there are actually two distinct paths for vortex annihilation: When a complete magnetic reversal takes place, a vortex enters on one side of a dot and exits out the opposite side. But if the magnetization is returned to its original orientation before a complete reversal has occurred, then the vortex will exit on the same side from which it has entered. We are unable to obtain a precise field value for this later path of annihilation; however, it is shown that, statistically, the vortex annihilates with greater ease when it exits out the same side from which it has entered. © *1999 American Institute of Physics.* [S0021-8979(99)08409-1]

I. INTRODUCTION

FORC diagrams are a powerful new method of investigating hysteresis in magnetic systems. We have used this method to study interactions in magnetic recording media[1] and multidomain behavior in geological samples.[2] Here, we apply the method to an array of polycrystalline Co dots produced by interference lithography. Small, lithographically patterned structures such as these have potential applications in the field of magnetic recording.[3,4] This array of Co dots presents an especially exciting system for a FORC diagram study, because the dots in this array reverse their magnetization through the nucleation and annihilation of a single-vortex state. With a FORC diagram, we should be able to obtain precise values for the nucleation and annihilation fields involved in magnetic reversal. As it turns out, however, the dynamics of this vortex are more complicated than expected; our results, described below, indicate that there are actually two distinct annihilation fields for any given dot.

II. THE SAMPLE

The sample in this study consists of an array of elliptical Co dots produced by interference lithography and a lift-off process. A detailed description of the fabrication process is provided in Ref. 5. A scanning electron micrograph of a small portion of the array is shown in Fig. 1. The dots have a 450 nm major axis, a 260 nm minor axis, and a thickness of 30 nm. Cobalt has strong crystalline anisotropy, but the grains that make up these dots are randomly oriented and smaller than the theoretical domain wall width. Hence, crystalline anisotropy largely cancels, and a uniaxial, in-plane, shape anisotropy dominates the magnetic behavior of these samples.[5]

When the applied field is aligned with the particle easy (long) axis, this sample has a remanence of $M_{rs}/M_s = 0.80$ and coercivity of 21.2 mT [Fig. 2(a)]. Magnetic force microscopy (MFM) investigations have shown that when a saturating field is aligned with the easy axis and removed, the dots relax into a uniformly magnetized, single domain state.[5] When the field is reversed and increased in the opposite direction, a single-vortex state will nucleate and then annihilate, leaving a negatively oriented particle. MFM investigations also show that there is some random variation from one dot to the next in the value of the nucleation and annihilation fields.[6] This variance can be attributed to irregularities in particle shape, size or chemistry. However, the most likely source of this variance is the random arrangement of grains within each particle.

On the major hysteresis loop, the fields where the slope has a local maximum provide estimates of the vortex nucleation and annihilation fields. For the applied field aligned with the particle easy axis [Fig. 2(a)], we obtain $H_N = -4.0$ mT and $H_A = 88.7$ mT. However, these estimates are not very accurate because, in addition to vortex nucleation and annihilation, the reversible movement of the vortices inside the dots is also contributing to the major hysteresis loop; there is no way of isolating just the contribution due to nucleation and annihilation events.

By contrast, since remanence curves are measured at zero field, vortex movement does not occur, and one is able to isolate the change in magnetization due to nucleation and annihilation events. We measured the isothermal remanent magnetization (IRM) and dc demagnetization remanence

[a)]Electronic mail: pike@geology.ucdavis.edu
[b)]Current address: Etec Systems, Inc., Hayward, CA 94545.

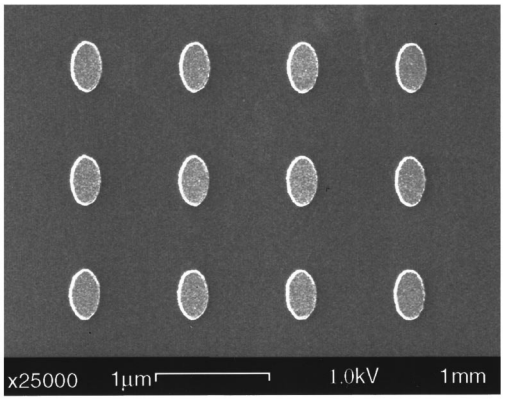

FIG. 1. A scanning electron micrograph of a portion of the Co dot array. The dots, which are produced by interference lithograph and a lift-off process, are nominally 450 nm×250 nm in size and 30 nm thick.

(DCD) remanence curves with the applied field aligned with the particle easy axis (Fig. 3). (The IRM remanence curve begins in a demagnetized state and the DCD curve begins in a negatively saturated state.) From these curves we estimate the vortex annihilation field at $H_A = 92.6$ mT. The nucleation field cannot be estimated from the IRM curve because all the particles begin in a vortex state, so no nucleation takes place. The DCD curve begins in a negative saturation state, so nucleation does take place, but it is difficult to discern where, in the neighborhood of $H=0$, this curve has a maximum slope; hence it is difficult to estimate H_N.

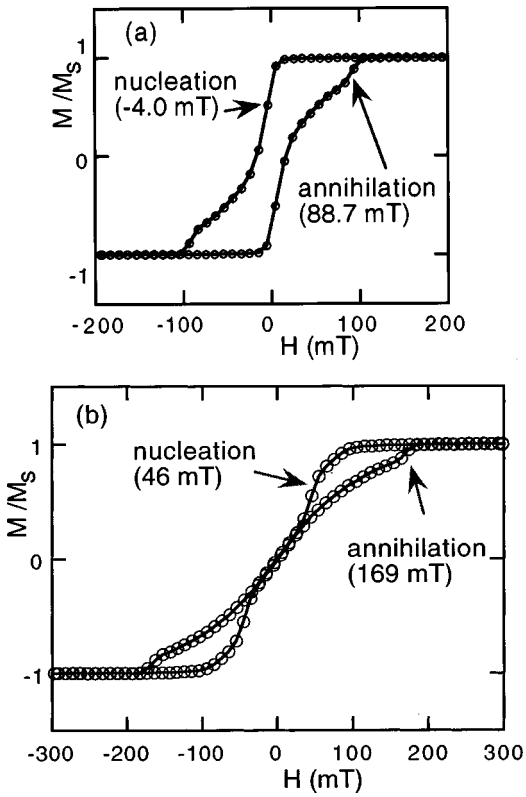

FIG. 2. Major hysteresis loop for field aligned with (a) easy and (b) hard particle axis. The values for nucleation and annihilation fields are only rough estimates.

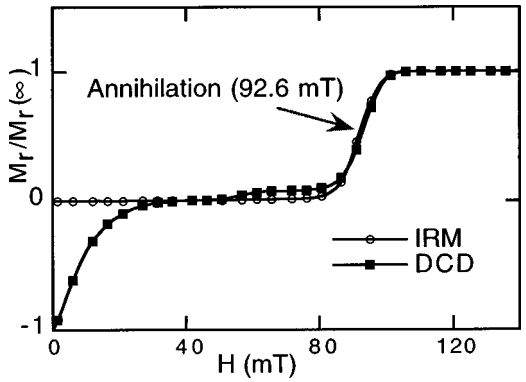

FIG. 3. IRM and DCD remanence curves for field aligned with easy particle axis. The annihilation field value is probably a better estimate than that given by the major hysteresis loop.

For the applied field aligned with the hard (short) axis, the hysteresis loop has negligible coercivity or remanence [Fig. 2(b)]. This is because when a saturating field is applied along the hard axis and removed, the particles relax into a single-vortex state, as shown by MFM investigations.[5] From the major hysteresis loop we estimate the median values: $H_N = 46$ mT and $H_A = 169$ mT. However, as described above, these estimates have considerable uncertainty. The IRM and DCD remanence curves are of no use when the applied field is aligned with the hard axis, since the remanent state is always a vortex state.

III. FORC DIAGRAMS

A FORC diagram is calculated from a class of hysteresis curves known as first order reversal curves. As shown in Fig. 4, the measurement of a FORC begins with the saturation of the sample by a large positive applied field. The field is then ramped down to a reversal field H_a. The FORC consists of a measurement of the magnetization as the applied field is increased from H_a back up to saturation. The magnetization at the applied field H_b on the FORC with reversal point H_a is denoted by $M(H_a, H_b)$, where $H_b \geq H_a$. A FORC distribution is defined as the mixed second derivative

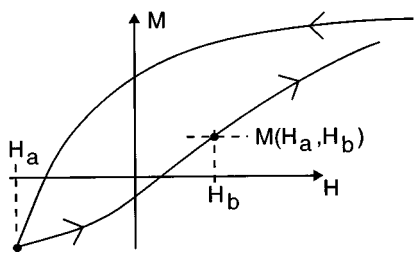

FIG. 4. Definition of a first order reversal curve. The measurement of a FORC begins by saturating the sample with a large positive applied field. The applied field is then decreased to a reversal field H_a. The FORC is comprised of a measurement of the magnetization as the applied field is increased from H_a back up to saturation. The magnetization at H_b on a FORC with reversal field H_a is denoted by $M(H_a, H_b)$, where $H_b \geq H_a$.

$$\rho(H_a,H_b) \equiv -\frac{\partial^2 M(H_a,H_b)}{\partial H_a \partial H_b}, \tag{1}$$

where this is well defined only for $H_b > H_a$.

When a FORC distribution is plotted, it is convenient to change coordinates from $\{H_a,H_b\}$ to $\{H_c \equiv (H_b - H_a)/2, H_u \equiv (H_a + H_b)/2\}$. A FORC diagram is a contour plot of a FORC distribution with H_c and H_u on the horizontal and vertical axes, respectively. Since $H_b > H_a$, we have $H_c > 0$, and a FORC diagram is confined to the right side half plane. As shown in Ref. 1, for a collection of noninteracting single-domain particles, H_c is equivalent to particle coercivity.

We have developed a procedure for calculating accurate FORC diagrams. A detailed description of this procedure can be found in Ref. 1. The smoothing factor, field spacing, and averaging time are parameters of the measurement and calculation procedure described in Ref. 1.

IV. EXPERIMENTAL RESULTS

We have investigated the FORC distribution of the Co dot array and found that it consists of three prominent features: two peaks, one in the upper half plane and one in the lower, and a ''butterfly'' structure on the central horizontal axis, which consists, roughly, of a circular region of negative values superimposed on an elongated horizontal region of positive values. Rather than displaying the full FORC distribution in one diagram, we have acquired FORC diagrams which focus in on these specific features. Each of the diagrams in this study required the separate measurement of 99 FORCs.

Figures 5–8 were acquired with the applied field aligned with the particle easy axis. Figure 5 includes both the upper and lower peaks in order to compare their height. The ratio of the upper to lower peak was 0.304. Because the lower peak is so much more pronounced, the upper peak does not show up well in Fig. 5. Figures 6 and 7 focus on the individual peaks. The field spacing for Figs. 6 and 7 was smaller than that of Fig. 5, giving them greater resolution. The coordinates of the lower and upper peaks were $\{H_c,H_u\} = \{49.3, -43.3 \pm 0.2\,\text{mT}\}$ and $\{47.8,\ 44.4 \pm 0.3\,\text{mT}\}$, respectively. Figure 8 focuses on the ''butterfly'' structure.

Figures 9–12 were acquired with the applied field aligned with the hard axis. Figure 9 includes both peaks; the ratio of upper to lower was 0.45. Figures 10 and 11 focus on the individual peaks, which have coordinates: $\{62.0, -105.3 \pm 0.5\,\text{mT}\}$ and $\{61.2,\ 107.2 \pm 0.3\,\text{mT}\}$. Figure 12 focuses on the butterfly structure.

V. HYSTERESIS MODELS

To help us interpret these FORC diagrams, we examine the following four, highly simplified models.

A. Square hysteresis loops

We will initially neglect all reversible changes in magnetization, and model the magnetic hysteresis of a particle as the sum of two square loops, as diagrammed in Fig. 13(a). In this diagram, the applied field begins at positive saturation. When the field falls bellow H_N, a vortex nucleates and the magnetization goes to zero. When the field falls below $-H_A$, this vortex will exit the particle out the opposite side from which it has entered; this is necessary to achieve a full reversal of the magnetization. If the applied field is reversed after the vortex has nucleated but before it has annihilated (i.e., before magnetic reversal has been completed), then when the field rises above H_A the vortex will exit out the same side from which it has entered; this is necessary in order for the magnetization to return to a positive orientation. Implicit in this model are these two inequalities: $-H_A < H_N$ and $H_N < H_A$.

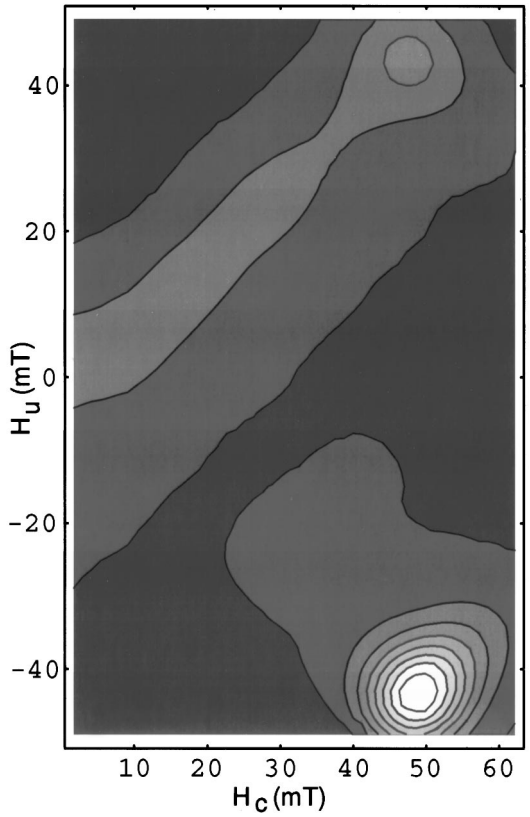

FIG. 5. FORC diagram for field aligned with easy axis, displaying both peaks: field spacing: 1.7 mT, smoothing factor: 5, averaging time: 1 s.

On a FORC curve, the magnetization of the model diagrammed in Fig. 13(a) can be written:

$$M(H_a,H_b) = \theta[H_b - H_N + (H_N - H_A)\,\theta(H_N - H_a)] - \theta[-H_A - H_b + (H_A - H_N)\,\theta(-H_A - H_a)], \tag{2}$$

where $\theta(x) = \{0 \text{ for } x < 0;\ 1 \text{ for } x > 0\}$. The upper square loop in Fig. 13(a) is represented by the first term in Eq. (2), and the lower loop by the second. Taking a derivative with respect to H_b we get

$$dM(H_a,H_b)/dH_b = \delta(H_b - H_N)\,\theta(H_a - H_N) + \delta(H_b - H_A)\,\theta(H_N - H_a) + \delta(H_b + H_A)\,\theta(H_a + H_A) + \delta(H_b + H_N)\,\theta(-H_A - H_a). \tag{3}$$

Taking the derivative with respect to H_a and multiplying by -1, we get

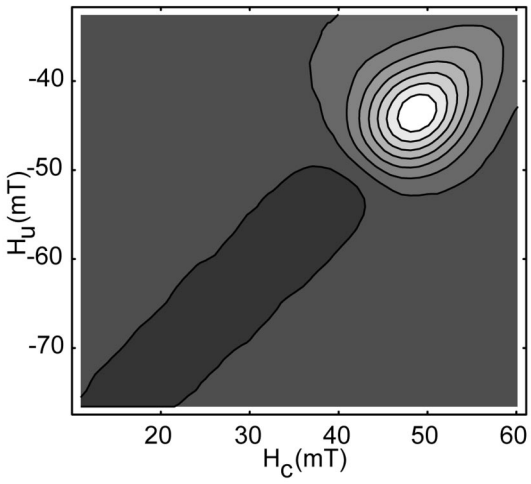

FIG. 6. Easy axis. Lower peak at {48.7, -43.3 ± 0.2 mT}: field spacing: 1.1 mT, smoothing factor: 5, averaging time: 1 s.

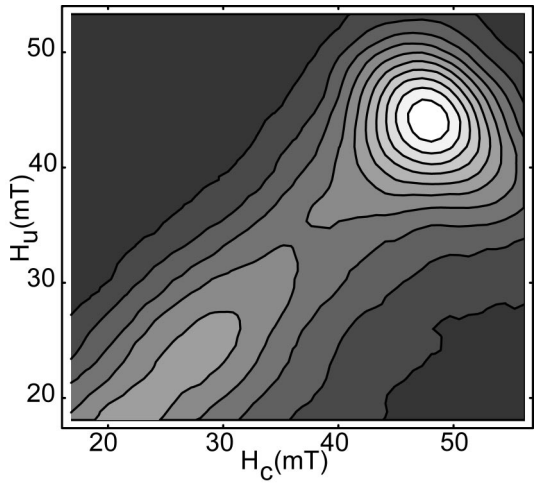

FIG. 7. Easy axis. Upper peak at {47.8, 44.2 ± 0.3 mT}: field spacing: 0.8 mT, smoothing factor: 7, averaging time: 1 s.

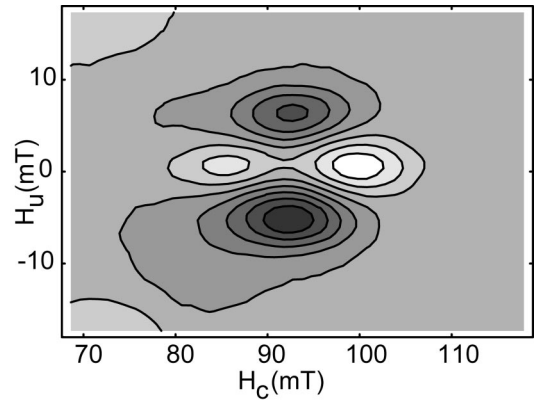

FIG. 8. Easy axis. Butterfly structure: field spacing: 0.9 mT, smoothing factor: 9, averaging time: 1 s.

$$\rho(H_a,H_b) = -\delta(H_b-H_N)\delta(H_a-H_N) + \delta(H_b-H_A)\delta(H_N-H_a) - \delta(H_b+H_A)\delta(H_a+H_A) + \delta(H_b+H_N)\delta(-H_A-H_a). \quad (4)$$

Since $H_b > H_a$, the first and third terms equal zero, so

$$\rho(H_a,H_b) = \delta(H_b-H_A)\delta(H_N-H_a) + \delta(H_b+H_N)\delta(H_A+H_a). \quad (5)$$

Changing variables to H_c and H_u, we get:

$$\rho(H_c,H_u) = \delta[H_c-(H_A-H_N)/2]\delta[H_u\pm(H_N+H_A)/2]. \quad (6)$$

Thus, on a FORC diagram we obtain two point delta functions, one in the upper quadrant and one in the lower, with coordinates $\{H_c,H_u\}=\{(H_A-H_N)/2, \pm(H_N+H_A)/2\}$. The H_c coordinate is equal to the square loop half width, and the H_u coordinates are equal to the offset of the square loop centers. Conversely, the nucleation and annihilation fields can be calculated from the coordinates of the point delta functions:

$$H_A = H_u + H_c; \quad H_N = H_u - H_c \quad (7a)$$

using the upper delta point, and

$$H_N = -H_c - H_u; \quad H_A = H_c - H_u \quad (7b)$$

using the lower delta point.

Since a real collection of particles will have variations in chemistry, size, shape and grain structure, these delta functions will be smoothed to some degree.

B. Curvilinear hysteresis loop

Next, we allow a vortex, once it has nucleated, to move reversibly inside a particle. This will be modeled by letting the bottom (top) branch of the upper (lower) hysteresis loop be curved as diagrammed in Fig. 13(b). On a FORC curve, the magnetization on the upper loop is

$$M_{\text{upper}}(H_a,H_b) = \theta[H_b-H_N+(H_N\text{-}H_A)\theta(H_N-H_a)] + f(H_b) \times\{1-\theta[H_b-H_N+(H_N-H_A)\theta(H_N-H_a)]\} \quad (8)$$

where $f(H)$ is the magnetization on the bottom branch of the upper loop and on the top branch of the lower loop. Evaluating the mixed derivative and multiplying by -1, we get

$$\rho_{\text{upper}}(H_a,H_b) = [1-f(H_A)]\delta(H_b-H_A)\delta(H_N-H_a) + [df(H_b/dH_b)]\delta(H_N-H_a)\theta(H_b-H_N) \times\theta(-H_b+H_A) - [df(H_b)/dH_b] \times\delta(H_N-H_a)\theta(H_N-H_b)\theta(H_b-H_A). \quad (9)$$

Since $H_N < H_A$, the third term in Eq. (9) is zero. The first term yields the same upper point delta function which we obtained in the previous section, but with a prefactor $[1-f(H_A)]$. The second term generates positive values at H_a

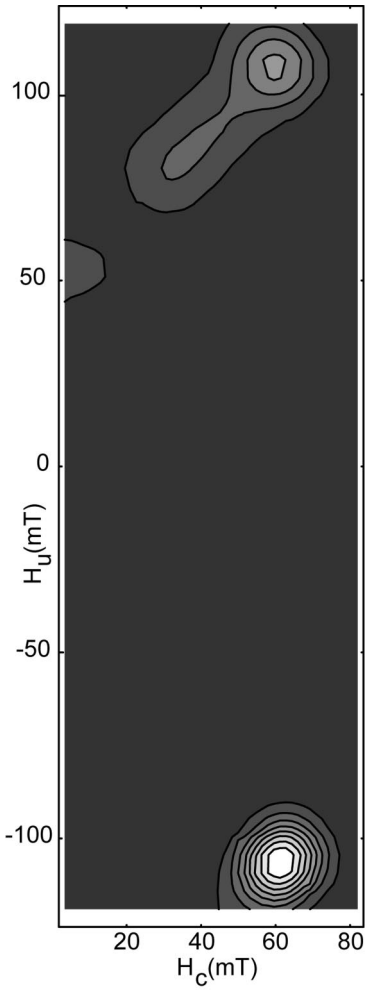

FIG. 9. Field aligned with hard axis. Both peaks: field spacing: 3.4 mT, smoothing factor: 4, averaging time: 0.5 s.

$=H_N$, for $H_N<H_b<H_A$. On a FORC diagram, this is a $+45°$ line between the upper point delta function and the $H_c=0$ axis.

The magnetization on the lower loop in Fig. 13(b) is

$$\begin{aligned} M_{\text{lower}}(H_a,H_b) &= -\theta[-H_A-H_b+(H_A-H_N)\theta(-H_A-H_a)] \\ &\quad -f(H_b)\{-1 \\ &\quad +\theta[-H_A-H_b+(H_A-H_N)\theta(-H_A-H_a)]\}. \end{aligned} \tag{10}$$

Evaluating the mixed derivative we get

$$\begin{aligned} \rho_{\text{lower}}(H_a,H_b) &= [1+f(-H_N)]\delta(H_b+H_N)\delta(H_a+H_A) \\ &\quad +[df(H_b)/dH_b]\delta(H_a+H_A)\theta(-H_A-H_b) \\ &\quad \times\theta(H_N+H_b)-[df(H_b)/dH_b] \\ &\quad \times\delta(H_a+H_A)\theta(H_A+H_b)\theta(-H_N-H_b). \end{aligned} \tag{11}$$

Since $H_N<H_A$, the second term in Eq. (11) is equal to zero. The first term yields the same lower point delta function which we obtained in Sec. V A, but with a prefactor $[1+f(-H_N)]$. The third term generates negative values at

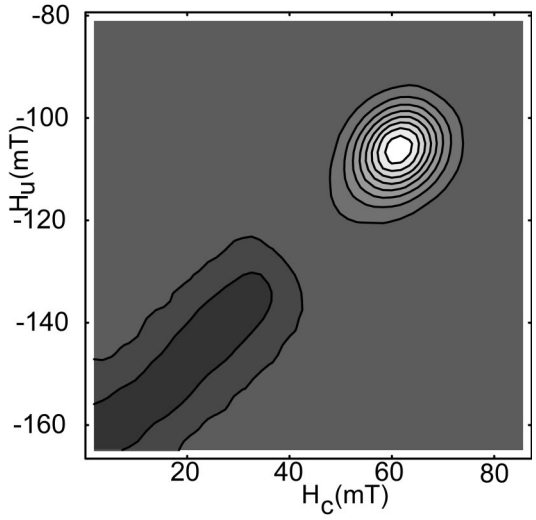

FIG. 10. Hard axis. Lower peak at $\{61.5, -106.0\pm0.5\ \text{mT}\}$: field spacing: 1.7 mT, smoothing factor: 5, averaging time: 0.4 s.

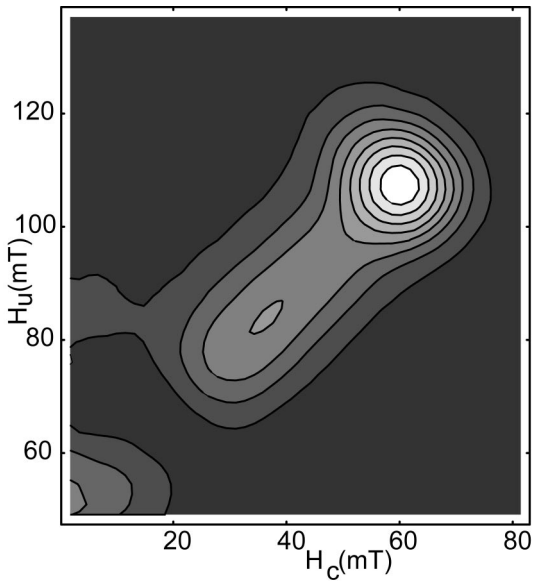

FIG. 11. Hard axis. Upper peak at $\{60.2, 107.2\pm0.3\ \text{mT}\}$: field spacing: 1.7 mT, smoothing factor: 7, averaging time: 0.6 s.

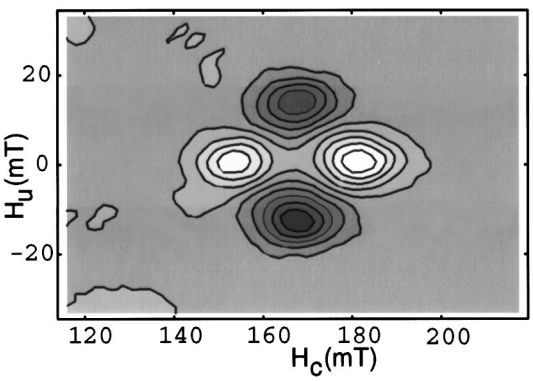

FIG. 12. Hard axis. Butterfly structure: field spacing: 1.7 mT, smoothing factor: 10, averaging time: 0.6 s.

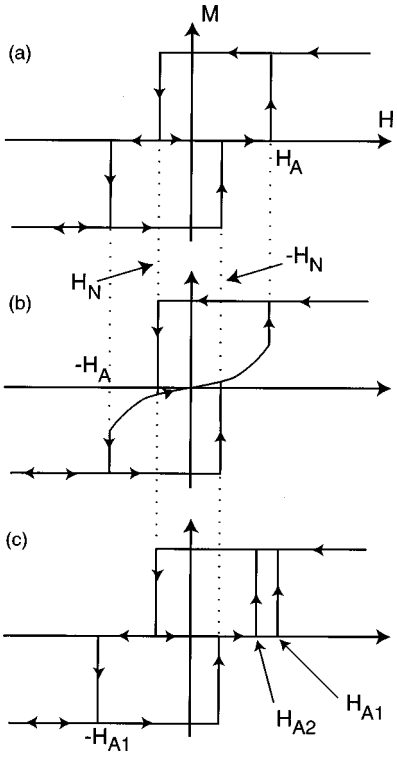

FIG. 13. Particle magnetization modeled by (a) two square loops, (b) two curvilinear loops, (c) two square loops with different annihilation fields.

$H_a = -H_A$, for $-H_A < H_b < -H_N$. On a FORC diagram, this is a $+45°$ line between the lower point delta function and the $H_c = 0$ axis.

In summary, because of reversible vortex movement, the ratio of the magnitude of the upper delta point function to the magnitude of the lower delta function is $[1-f(H_A)]/[1+f(-H_N)]$. It can be seen from Fig. 13(b) that this is less than one; so the lower peak has a greater magnitude than the upper peak. Reversible movement also results in positive (negative) values on a $+45°$ line between the upper (lower) point delta function peak and the $H_c = 0$ axis.

C. Two uncorrelated annihilation fields

It can be expected that particle irregularities such as grain texture will play a role in the nucleation and annihilation of vortices. Hence, there will be one site on a particle where vortex nucleation is favored. As mentioned earlier, there are actually two paths for vortex annihilation: a vortex can exit a dot out the same side from which it has entered, or out the opposite side. Due to irregularities, these two different paths will have two different annihilation fields for an individual particle. We therefore generalize our model to include two distinct annihilation fields, as diagrammed in Fig. 13(c). We define H_{A1} as the annihilation field when annihilation takes place on the opposite side of nucleation, and H_{A2} as the annihilation field when annihilation takes place on the same side. Implicit in this model are the inequalities: $H_N < \{H_{A1}, H_{A2}\}$ and $H_N > \{-H_{A1}, -H_{A2}\}$.

On a FORC the hysteresis behavior diagrammed in Fig. 13(c) can be expressed as:

$$\begin{aligned} M(H_a, H_b) &= \theta[H_b - H_N + (H_N - H_{A2})\,\theta(H_N - H_a) \\ &\quad + (H_{A2} - H_{A1})\,\theta(-H_{A1} - H_a)] \\ &\quad - \theta[-H_{A1} - H_b + (H_{A1} - H_N)\,\theta(-H_{A1} - H_a)]. \end{aligned} \tag{12}$$

In Appendix A, the mixed second derivative of Eq. (12) is evaluated. The resulting expression is

$$\begin{aligned} \rho(H_a, H_b, H_N, H_{A1}, H_{A2}) &= \delta(H_b - H_{A2})\,\delta(H_N - H_a)\,\theta(H_{A1} + H_a) \\ &\quad - \delta(H_b - H_{A2})\,\theta(H_N - H_a)\,\delta(H_{A1} + H_a) \\ &\quad + \delta(H_b - H_{A1})\,\delta(-H_{A1} - H_a) \\ &\quad + \delta(H_b + H_N)\,\delta(-H_{A1} - H_a). \end{aligned} \tag{13}$$

Next, let us consider a collection of particles with a statistical distribution of nucleation and annihilation fields. Here, we will treat the two annihilation fields, H_{A1} and H_{A2}, as independent variables which have the same statistical distribution. That is, the values of H_{A1} and H_{A2} for a given particle will not be correlated, but over the collection of particles they will have the same statistical distribution. To simplify the analysis it is advantageous to write the distribution of particles as the product of three distributions: $\rho_N(H_N)\rho_A(H_{A1})\rho_A(H_{A2})$, where ρ_N denotes the distribution of nucleation fields and ρ_A denotes the distribution of annihilation fields. This is not generally possible because of the inequalities $H_N < \{H_{A1}, H_{A2}\}$ and $H_N > \{-H_{A1}, -H_{A2}\}$. However, if it is assumed that $\rho_N(x)$ is distributed at smaller values than $\rho_A(x)$, with no overlap, then the first constraint will always be satisfied. Similarly, if it is assumed that $\rho_N(x)$ is distributed at larger values than $\rho_A(-x)$, again with no overlap, then the second constraint will always be satisfied. We can then write the distribution of particles as the above described product.

$\rho(H_a, H_b)$ is obtained by integrating $\rho(H_a, H_b, H_N, H_{A1}, H_{A2})$ in Eq. (13) over these distributions. This integration is done in Appendix A. The result is

$$\begin{aligned} \rho(H_a, H_b) &= \int\int\int_{-\infty,\infty} dH_N\, dH_{A1}\, dH_{A2}\, \rho_N(H_N)\rho_A(H_{A1}) \\ &\quad \times \rho_A(H_{A2})\,\rho(H_a, H_b, H_N, H_{A1}, H_{A2}) \end{aligned} \tag{14}$$

$$\begin{aligned} &= \rho_N(H_a)\rho_A(H_b) - \rho_A(-H_a)\rho_A(H_b) \\ &\quad + \rho_A(H_b)\,\delta(H_a + H_b) + \rho_N(-H_b)\rho_A(-H_a). \end{aligned} \tag{15}$$

The first and last terms generate peaks in the upper and lower quadrants of a FORC diagram. The two middle terms, however, give rise to a new feature: a butterfly structure on the central horizontal axis. This butterfly structure is a consequence of the presence of two uncorrelated annihilation fields. To illustrate the general features of the model, we have changed variables and calculated a FORC diagram of $\rho(H_c, H_u)$ using Gaussian functions for ρ_N and ρ_A, with means of 0.2 and 2.0, respectively, and standard deviations of 0.43 (Fig. 14).

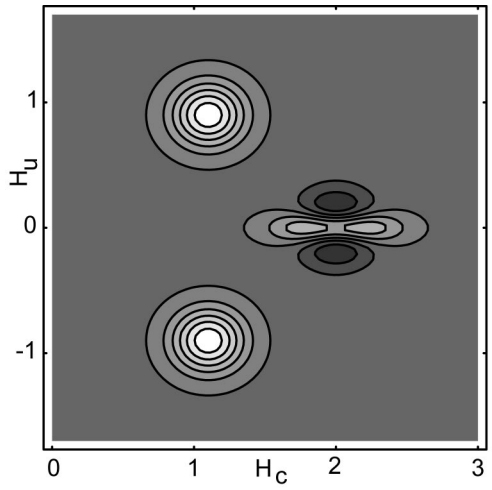

FIG. 14. FORC diagram for two uncorrelated annihilation fields having identical distributions. Calculated using Eq. (15). ρ_N and ρ_A have means 0.2 and 2.0, respectively, and standard derivations of 0.42.

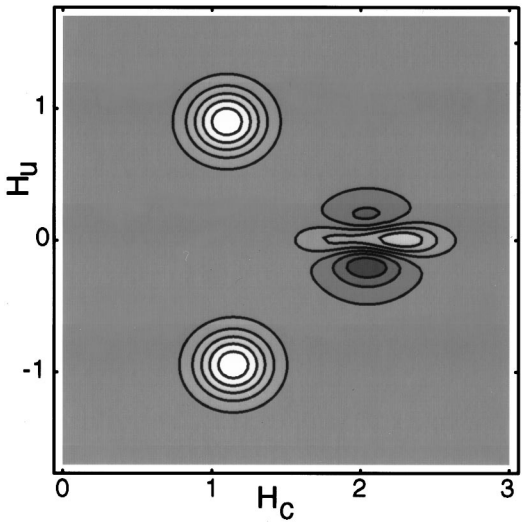

FIG. 15. FORC diagram calculated using Eq. (17) with $k=0.09$, where ρ_N and ρ_{A1} have means 0.2 and 2.0, respectively, and standard derivations of 0.42, and where the distribution of H_{A2} is given by $\rho_{A1}(H_{A2}+k)$.

D. Two annihilation fields; H_{A2} distributed at smaller values

In Sec. V C, it was assumed that the two annihilation field values, H_{A1} and H_{A2}, had the same statistical distribution. But in actuality, a distinction between these two distributions is expected for the following reason: When a vortex nucleates, it will pick that site on the particle surface where irregularities cause the greatest reduction in the nucleation energy barrier. It is reasonable to assume that the same irregularities which lower the energy barrier to vortex nucleation will also lower the energy barrier to vortex annihilation. Therefore, the location on the particle where vortex nucleation takes place will also tend to be a favorable location for vortex annihilation. Since H_{A2} is defined as the annihilation field when a vortex exits on the same side it enters, then it follows that H_{A2} will tend to be smaller than H_{A1}.

To model this effect, we shift the distribution of H_{A2} to smaller values. We will write the distribution of H_{A1} as $\rho_{A1}(H_{A1})$ and the distribution of H_{A2} as $\rho_{A1}(H_{A2}+k)$ where k is positive. Then Eq. (14) becomes

$$\rho(H_a,H_b)=\int\int\int_{-\infty,\infty} dH_N\,dH_{A1}\,dH_{A2} \times\rho_N(H_N)\rho_{A1}(H_{A1})\rho_{A1}(H_{A2}+k) \times\rho(H_a,H_b,H_N,H_{A1},H_{A2}). \tag{16}$$

This integration is evaluated in Appendix A. We get

$$\rho(H_a,H_b) =\rho_N(H_a)\rho_{A1}(H_b+k) -\rho_{A1}(-H_a)\rho_{A1}(H_b+k)+\rho_{A1}(H_b)\delta(H_a+H_b) +\rho_N(-H_b)\rho_{A1}(-H_a). \tag{17}$$

The last term in Eq. (17) generates a peak in the lower quadrant of a FORC diagram. This peak will be located at $H_a=-\langle H_{A1}\rangle$ and $H_b=-\langle H_N\rangle$, where $\langle H_N\rangle$ and $\langle H_{A1}\rangle$ denote the medians of the distributions of H_N and H_{A1}, respectively. On a FORC diagram, after changing variables to H_c and H_u, this lower peak will have coordinates $\{H_c,H_u\}=\{(\langle H_{A1}\rangle-\langle H_N\rangle)/2,-(\langle H_{A1}\rangle+\langle H_N\rangle)/2\}$. Conversely, we can calculate $\langle H_N\rangle$ and $\langle H_{A1}\rangle$ from the coordinates of the lower peak:

$$\langle H_N\rangle=-H_c-H_u;\quad \langle H_{A1}\rangle=H_c-H_u \tag{18a}$$

The first term in Eq. (17) generates a peak in the upper quadrant. This peak will be located at $H_a=\langle H_N\rangle$ and $H_b=\langle H_{A1}\rangle-k$. Since $\rho_{A1}(H_{A2}+k)$ is the distribution of the annihilation field H_{A2}, we can write $\langle H_{A2}\rangle+k=\langle H_{A1}\rangle$, so $H_b=\langle H_{A2}\rangle$. On a FORC diagram, after changing variables to H_c and H_u, this upper peak will have coordinates $\{(\langle H_{A2}\rangle-\langle H_N\rangle)/2,\ (\langle H_{A2}\rangle+\langle H_N\rangle)/2\}$. Conversely, we can calculate $\langle H_N\rangle$ and $\langle H_{A2}\rangle$ from the coordinates of the upper peak:

$$\langle H_N\rangle=H_u-H_c;\quad \langle H_{A2}\rangle=H_u+H_c. \tag{18b}$$

To illustrate the features of this model, we changed variables and calculated a FORC diagram of $\rho(H_c,H_u)$ for $k=0.09$ using the distribution functions of Sec. V. C and letting $\rho_{A1}=\rho_A$. As seen in Fig. 15, the negative region of the butterfly structure has been shifted leftward and downward relative to the positive region.

VI. COMPARISON OF THEORY AND EXPERIMENT

On the basis of the above-described models, we can identify the peaks in our FORC diagrams as manifestations of the nucleation and annihilation of single-vortex states. The presence of the butterfly structures in Figs. 8 and 12 is consistent with the model of Sec. V C and is an indication that there are two distinct annihilation processes. The region of positive values contained in this butterfly structure is shifted to the left and downward relative to the region of negative values. This is most evident when the applied field is aligned with the particle easy axis (Fig. 8). This shift is consistent

with the results of the model in Sec. V D and indicates that the median value of H_{A2} is less than that of H_{A1}. In other words, a vortex is annihilated with greater ease when it exits out the same side from which it has entered.

We have also observed a region of positive values on a $+45°$ line between the upper peak and the $H_c=0$ axis (Figs. 7 and 11), and a region of negative values on a $+45°$ line between the lower peak and the $H_c=0$ (Figs. 6 and 10). These features are consistent with the model in Sec. V B and can be identified as manifestations of the reversible movement of the vortices. In addition, it has been found that the upper peak has a smaller magnitude than the lower peak (Figs. 5 and 9). In Sec. V B, this was also shown to be a manifestation of reversible vortex movement. In the case of the particular sample studied here, the reversible movement of the vortex is large enough that it has reduced the magnitude and clarity of the upper peaks, particularly when the field is aligned with the easy axis (Fig. 5). It appears that there is greater reversible movement when the applied field is aligned with the easy axis.

Using Eq. (18b), the median value of the vortex nucleation field can be calculated from the coordinates of the upper peak. For the applied field aligned with the particle easy axis, and with the coordinates of the upper peak from Fig. 7, we get $\langle H_N\rangle=-3.6\pm0.5$ mT. Using Eq. (18a), the median annihilation field H_{A1} can be calculated from the coordinates of the lower peak. With the coordinates of the lower peak from Fig. 6, we get $\langle H_{A1}\rangle=92.0\pm0.4$ mT.

For the applied field aligned with the hard axis, and using the peaks in Figs. 10 and 11, the same calculation gives us $\langle H_N\rangle=47.0\pm0.8$ mT and $\langle H_{A1}\rangle=167.5\pm0.8$ mT. Hence, when the applied field is aligned with the hard axis, the vortex nucleates with greater ease, and annihilates with greater difficulty. The different nucleation and annihilation fields associated with the two orientations can be qualitatively explained as being due to the different demagnetization fields.[7]

In the model of Sec. V D, expressions were also derived to calculate $\langle H_N\rangle$ from the lower peak and $\langle H_{A2}\rangle$ from the upper peak. Unfortunately, the reversible movement of the vortex invalidates these calculations. For example, the annihilation event at H_{A2} in Fig. 13(c) will be preceded by a reversible increase in magnetization. On a FORC diagram, this reversible increase generates positive values on a $+45°$ line from the $H_c=0$ axis to the upper peak. The upper peak will be superimposed upon this $+45°$ line. This causes an apparent shift in the peak's location downward and to the left along a $+45°$ line, which skews an estimate of $\langle H_{A2}\rangle$ towards reduced values.

The peaks in these FORC diagrams have considerable spread. This indicates that there is a variance in the nucleation and annihilation field values among the collection of particles. We attribute this variance to the random arrangement of grains within a particle. We can quantify the variance of the nucleation field H_N by taking the 1/2 width of a cross section at a $-45°$ angle through the upper peak on a FORC diagram. For the field aligned with the easy axis, we calculated the 1/2 width of the H_N distribution to be 8.4 mT. MFM measurements of a similar dot array have shown that there is a variance in nucleation fields of 7.5 mT. This corresponds to a 1/2 width of 8.8 mT, in excellent agreement with the value obtained here.[6]

[There is a question of how much of the spread on a FORC diagram is real and how much is due to numerical effects. It can be shown that a feature of a FORC diagram which would have a length equal to (1+2*smoothing factor)*(field spacing) in the absence of numerical effects, will be increased in length by 8% on a FORC diagram calculated numerically from data; larger features will be increased by smaller fractions. In the numerical calculation just described, field spacing=0.8 mT, smoothing factor=2, and (1+2*smoothing factor)*(field spacing)=4 mT, which is considerably smaller than the calculated peak 1/2 width of 8.4 mT. Therefore, we can conclude that this spread is, to a good approximation, due to variance in the underlying particle nucleation fields.]

VII. CONCLUSIONS

These FORC diagrams indicate that there are actually two distinct paths of vortex annihilation: the vortex can exit out the opposite side of the particle from which it has entered, or it can exit out the same side. The former completes a particle's magnetic reversal, the latter returns a particle to its original magnetic orientation. Within an individual particle, these two paths can have different annihilation field values; we attribute this to the effect of grain texture. Using a FORC diagram, we have obtained precise median values for the nucleation field and for the annihilation field (i.e., H_{A1}) associated with a magnetic reversal. These values are much more precise than can be obtained via the major hysteresis loop or remanence curves. However, we were unable to obtain a precise value for the annihilation field associated with returning a particle to its original orientation (i.e., H_{A2}); it was not possible to decouple this annihilation event from the reversible movement of the vortices. We were able to show, however, that the H_{A2} is statistically smaller than H_{A1}. In other words, annihilation tends to occur more easily when the vortex exists out the same side from which it has entered. This indicates that the same grain texture which promotes the nucleation of a vortex also promotes its annihilation.

ACKNOWLEDGMENTS

The authors are grateful to Dr. Kenneth Verosub of the Geology department at U. C. Davis for giving them use of his facilities.

APPENDIX A

Taking the derivative of Eq. (12) with respect to H_b,

$$\begin{aligned} dM(H_a,H_b)/dH_b=&\,\delta(H_b-H_N)\,\theta(-H_N+H_a)\,\theta(H_{A1}+H_a)\\ &+\delta(H_b-H_{A2})\,\theta(H_N-H_a)\,\theta(H_{A1}+H_a)\\ &+\delta(H_b-H_{A1})\,\theta(H_N-H_a)\,\theta(-H_{A1}-H_a)\\ &+\delta(H_b+H_{A1})\,\theta(H_{A1}+H_a)\\ &+\delta(H_b+H_N)\,\theta(-H_{A1}-H_a). \end{aligned} \tag{A1}$$

Since $-H_{A1}<H_N$, then $\theta(-H_N+H_a)\theta(H_{A1}+H_a)=\theta(H_a-H_N)$ and $\theta(H_N-H_a)\theta(-H_{A1}-H_a)=\theta(-H_{A1}-H_a)$. Taking the derivative with respect to H_a and multiplying by -1 we get

$$\begin{aligned}\rho(H_a,H_b,H_N H_{A1},H_{A2}) &= -\delta(H_b-H_N)\delta(H_a-H_N)\\ &\quad+\delta(H_b-H_{A2})\delta(H_N-H_a)\theta(H_{A1}+H_a)\\ &\quad-\delta(H_b-H_{A2})\theta(H_N-H_a)\delta(H_{A1}+H_a)\\ &\quad+\delta(H_b-H_{A1})\delta(-H_{A1}-H_a)\\ &\quad-\delta(H_b+H_{A1})\delta(H_a+H_{A1})\\ &\quad+\delta(H_b+H_N)\delta(-H_{A1}-H_a). \qquad \text{(A2)}\end{aligned}$$

Since $H_b>H_a$, then the first and fifth terms are zero. After omitting these terms, we get Eq. (13).

Next, to evaluate Eq. (14) we integrate $\rho(H_a,H_b,H_N,H_{A1},H_{A2})$ in Eq. (13) over the distributions of H_N, H_{A1} and H_{A2}. We will perform this integration on the four terms of Eq. (13) one at a time:

(first term)

$$\begin{aligned}&\int_{-\infty}^{\infty} dH_N\, dH_{A1}\, dH_{A2}\rho_N(H_N)\rho_A(H_{A1})\rho_A(H_{A2})\\ &\quad\times\delta(H_b-H_{A2})\delta(H_N-H_a)\theta(H_{A1}+H_a)\\ &=\rho_N(H_a)\rho_A(H_b)\int_{-\infty}^{\infty} dH_{A1}\rho_A(H_{A1})\theta(H_{A1}-H_a)\\ &=\rho_N(H_a)\rho_A(H_b).\end{aligned}$$

The last step uses the fact that, since $\rho_N(x)$ is distributed at smaller values than $\rho_A(x)$ with no overlap, then $\rho_N(H_a)\rho_A(H_{A1})$ will equal zero whenever $H_{A1}<H_a$, and therefore the step function can be equated with 1.

(second term)

$$\begin{aligned}&-\int\int\int_{-\infty,\infty} dH_N\ldots\rho_A(H_{A2})\\ &\quad\times\delta(H_b-H_{A2})\theta(H_N-H_a)\delta(H_{A1}+H_a)\\ &=-\rho_A(-H_a)\rho_A(H_b)\int_{-\infty}^{\infty} dH_N\rho_N(H_N)\theta(H_N-H_a)\\ &=-\rho_A(-H_a)\rho_A(H_b).\end{aligned}$$

The last step uses the fact that, since $\rho_N(x)$ is distributed at larger values than $\rho_A(-x)$ with no overlap, then $\rho_A(-H_a)\rho_N(H_N)$ will equal zero whenever $H_N<H_a$, and the step function can be equated with 1.

(third term)

$$\begin{aligned}&\int\int\int_{-\infty,\infty} dH_N\ldots\rho_A(H_{A2})\delta(H_b-H_{A1})\delta(-H_{A1}-H_a)\\ &=\rho_A(H_b)\delta(H_a+H_b).\end{aligned}$$

(fourth term)

$$\begin{aligned}&\int\int\int_{-\infty,\infty} dH_N\ldots\rho_A(H_{A2})\delta(H_b+H_N)\delta(-H_{A1}-H_a)\\ &=\rho_N(-H_b)\rho_A(-H_a).\end{aligned}$$

Summing these four terms, we get Eq. (15).

Next, to evaluate Eq. (16) we replace $\rho_A(H_{A1})$ with $\rho_{A1}(H_{A1})$ and $\rho_A(H_{A2})$ with $\rho_{A1}(H_{A2}+k)$. Following the same steps taken above, we get:

(first term) $\rho_N(H_a)\rho_{A1}(H_b+k)$.

(second term) $-\rho_N(-H_a)\rho_{A1}(H_b+k)$.

(third term) $\rho_{A1}(H_b)\delta(H_b+H_a)$.

(fourth term) $\rho_N(-H_b)\rho_{A1}(-H_a)$.

Summing these four terms gives us Eq. (17).

[1] C. R. Pike, A. P. Roberts, and K. L. Verosub, J. Appl. Phys. **85**, 6660 (1999).
[2] C. R. Pike, A. P. Roberts, and K. L. Verosub, J. Geophys. Res. (submitted).
[3] L. Kong, L. Zhuang, and S. Y. Chou, IEEE Trans. Magn. **MAG-33**, 3019 (1997).
[4] R. M. New, R. F. W. Pease, and R. L. White, J. Magn. Magn. Mater. **155**, 140 (1996).
[5] A. Fernandez, M. R. Gibbons, M. A. Wall, and C. J. Cerjan, J. Magn. Magn. Mater. **190**, 71 (1998).
[6] A. Fernandez and C. J. Cerjan, J. Appl. Phys. (submitted).
[7] W. Wernsdorpher *et al.*, Phys. Rev. B **53**, 3341 (1996).